Current Applied Science and Technology e-ISSN: 2586-9396

Curr. Appl. Sci. Technol. ….., Vol... (No...), e0270910

Research article

Formulation and Optimization of Curcumin-Loaded Chitosan Nanoparticles: A Systematic Study of Solubility Enhancement and Physicochemical Characterization

Chayut Fongsuk[1], Chutwadee Krisanapun[2] and Duangratana Shuwisitkul[1]*

[1]Department of Pharmaceutical Technology, Faculty of Pharmacy, Srinakharinwirot University, Ongkharak Campus, Nakhon Nayok, 26120, Thailand
[2]Department of Biopharmacy, Faculty of Pharmacy, Srinakharinwirot University, Ongkharak Campus, Nakhon Nayok, 26120, Thailand

Received: 22 February 2026, Revised: 18 May 2026, Accepted: 15 June 2026, Published: 8 September 2026

Abstract

Curcumin, a polyphenolic compound derived from turmeric, has significantly therapeutic potential through its anti-inflammatory, antioxidant, and antimicrobial properties. However, its clinical application is severely limited by its poor aqueous solubility and low oral bioavailability. This study systematically evaluated the formulation and optimization of curcumin-loaded chitosan nanoparticles (CRCSNPs) via ionic gelation to overcome the limitations. Using a one-factor-at-a-time approach, critical parameters—including chitosan-to- sodium tripolyphosphate (TPP) mass ratio, pH, and curcumin loading—were methodically evaluated to identify optimal formulation conditions. The results demonstrated that a chitosan-to-TPP ratio of 4:1 at pH 5.0 with 5% w/w curcumin loading produced nanoparticles with a mean size of 211.9±10.6 nm and encapsulation efficiency of 96.88%. Fourier-transform infrared spectroscopy confirmed successful ionic crosslinking and specific interactions between curcumin and chitosan. Additionally, CRCSNPs achieved a 2.0-fold solubility enhancement in acetate buffer pH 4.5 and up to 2.8-fold enhancement in the presence of surfactants in comparison to free curcumin. Nanoparticle tracking analysis revealed a modal size of 162.5 nm, corroborating the dynamic light scattering data and supporting the presence of a well-dispersed nanoparticle population. These findings suggest a rational formulation strategy that supports improvements in curcumin's biopharmaceutical properties, offering further possibilities for pharmaceutical, nutraceutical, and cosmeceutical applications The systematic optimization approach provides a reproducible method for other poorly water-soluble bioactive compounds. Optimizing the chitosan-to-TPP ratio, pH, and curcumin loading allows for the fine-tuning of ionic crosslinking and hydrogen bonding. This results in a stable nanoparticle matrix that directly supports the improved solubility of the drug.

Keywords: chitosan; nanoparticles; curcumin; ionic gelation; solubility enhancement

*Corresponding author: E-mail: duangrats@g.swu.ac.th
https://doi.org/10.55003/cast.2026.270910

1. Introduction

Curcumin, a bioactive polyphenol derived from *Curcuma longa*, exhibits beneficial anti-inflammatory, antioxidant, antimicrobial, and metabolic effects, which demonstrate its broad therapeutic potential (Amalraj et al., 2017; Hewlings & Kalman, 2017). However, its clinical and industrial application is significantly limited by its low aqueous solubility (approximately 11 ng/mL), inherent chemical instability particularly characterized by rapid hydrolytic and oxidative degradation at physiological pH, and substantial first-pass metabolism, leading to an oral bioavailability of less than 1% (Anand et al., 2007). The significant challenges caused by poor biopharmaceutical properties require the development of highly efficient delivery systems that facilitate the effective incorporation of curcumin into nutraceutical, cosmeceutical, and pharmaceutical products (Urošević et al., 2022).

Polymeric nanoparticles have been widely studied as effective vehicles for solving the solubility and stability challenges associated with hydrophobic bioactive compounds (Gera et al., 2017; Urošević et al., 2022). Chitosan, a cationic polysaccharide obtained from the deacetylation of chitin, exhibits exceptional functional properties such as biocompatibility, biodegradability, muco-adhesiveness, pH-responsive behavior, and the capacity to regulate epithelial tight junctions (Dash et al., 2011; Ahsan et al., 2018). Chitosan nanoparticles (CSNPs) exhibit precisely adjustable physicochemical characteristics, including particle size, surface morphology, and crosslinking density, enabling the effective encapsulation of lipophilic compounds such as curcumin (Sogias et al., 2008; Ali & Ahmed, 2018). For this reason, CSNPs function as adaptable intermediate nanocarriers suitable for incorporation into various pharmaceutical and nutraceutical formulations.

Chitosan-based nanoparticles have effectively been utilized for a wide range of poorly water-soluble natural products, consistently enhancing apparent solubility, providing protection against degradation, and improving dispersibility in aqueous environments (Ahsan et al., 2018; Urošević et al., 2022). For instance, quercetin-loaded lecithin–chitosan nanoparticles, combined with other chitosan-based quercetin systems, exhibit superior physicochemical stability, sustained release, and enhanced biological activity when compared to free quercetin, which has limitations because of low water solubility and rapid degradation (Tan et al., 2011). Chitosan-modified nanocarriers similarly stabilize carotenoids such as β-carotene, enhancing their resistance to light and oxidative stress while facilitating their incorporation into aqueous food or supplement matrices (Bockuviene & Sereikaite, 2020). Essential oil components, such as thymol and thyme essential oil, have been encapsulated in chitosan nanoparticles, resulting in controlled release and enhanced antimicrobial effects against foodborne and phytopathogenic microorganisms compared to non-encapsulated oils (Granata et al., 2021; Kowalczyk et al., 2024). These examples together demonstrate the important advantages of chitosan-based nanoparticles as a versatile nanoplatform for encapsulating hydrophobic bioactives from natural sources. When designed as ready-to-use intermediates, these systems enable smooth incorporation into advanced cosmetic and nutraceutical formulations, thus simplifying the transition from laboratory-scale development to industrial application.

Curcumin-loaded CSNPs have been investigated extensively for their ability to enhance the solubility, chemical stability, and bioaccessibility of curcumin (Anitha et al., 2012). Nevertheless, existing optimization strategies remain notably varied and fragmented (Walbi et al., 2022). A significant proportion of current literature relies on empirical, trial-and-error methodologies, lacking a systematic and transparent elucidation

of how critical formulation parameters (CFPs)—including chitosan molecular weight, degree of deacetylation, chitosan-to-TPP mass ratio, pH, and stirring kinetics—influence nanoparticle architecture and the subsequent dissolution profiles of curcumin. Furthermore, there is a paucity of mechanistic insights regarding solubility enhancement; specifically, molecular-level characterization of curcumin–chitosan intermolecular interactions via techniques such as FTIR remains underdeveloped, despite its necessity for rational formulation design.

This study focused on the systematic formulation and optimization of curcumin-loaded chitosan nanoparticles (CRCSNP), primarily demonstrating solubility enhancement and essential physicochemical properties. The evaluation of critical process and formulation parameters—such as chitosan-to-TPP ratio, pH, stirring kinetics, and curcumin loading—was conducted systematically using a rational one-factor-at-a-time (OFAT) approach. This method was utilized to identify major trends and establish optimal ranges for each parameter. This method was selected to provide a clear and straightforward assessment of individual factors during the initial formulation stages. The fundamental principles of solubility enhancement were clarified through the characterization of intermolecular interactions between curcumin and the chitosan matrix via FTIR spectroscopy. A comprehensive evaluation of particle size, zeta potential, encapsulation efficiency, and release-related behavior was conducted to identify optimized formulations that effectively balanced curcumin solubility and favorable dispersion characteristics. This study presents a reliable and mechanistically informed nanoplatform for the effective incorporation of curcumin and similar hydrophobic bioactives into advanced cosmetic and nutraceutical systems.

2. Materials and Methods

2.1 Chemicals and materials

Curcumin (purity ≥95% by HPLC) was purchased from Sigma-Aldrich (St. Louis, MO, USA). Low-molecular weight chitosan (LMW-CS; 5–20 mPa·s, 0.5% in 0.5% acetic acid at 20 °C, degree of deacetylation [DD] 75–85%) was supplied from TCI (Japan). Sodium tripolyphosphate (TPP, analytical grade), methanol, dimethyl sulfoxide (DSMO), hydrochloric acid 37% fuming AR (HCl) and glacial acetic acid (99.7%) were obtained from Merck KGaA (Darmstadt, Germany). Sodium lauryl sulfate (SLS) and Tween 20 were obtained from Kemaus (Australia). Potassium phosphate monobasic, potassium phosphate dibasic, sodium acetate trihydrate, and acetic acid were used to prepare phosphate and acetate buffers. All aqueous solutions were prepared with ultrapure water (18.2 MΩ·cm) produced by a Milli-Q system (Merck Millipore, Billerica, MA, USA). Cellulose acetate membrane filter (0.45 µm) and Amicon Ultra-15 centrifugal filter units with Ultracel-10 membrane (MWCO = 10 kDa) were used during sample preparation and analysis.

2.2 Preparation of curcumin-loaded chitosan nanoparticles

Curcumin-loaded chitosan nanoparticles (CRCSNPs) were synthesized via ionic gelation, a well-established technique based on electrostatic interactions between the cationic amino groups of chitosan and the anionic phosphate groups of sodium tripolyphosphate (TPP) (Amalraj et al., 2017; Hewlings & Kalman, 2017). Chitosan was dissolved in 1% v/v acetic acid at concentrations ranging from 0.5 to 1.5 mg/mL and allowed to equilibrate for 24 h at room temperature to ensure complete dissolution. Sodium tripolyphosphate solution

(1.0-20.0 mg/mL) was prepared separately in ultrapure water. For curcumin-loaded formulations, curcumin (5-20% w/w relative to chitosan) was initially dissolved in absolute DMSO and added dropwise to the chitosan solution while stirring at 1000 rpm for 15 min using a magnetic stirrer (IKA, Germany) with a Teflon-coated stir bar to ensure uniform dispersion throughout the polymer matrix.

The TPP solution was then added dropwise at a controlled rate of 2 mL/min to the curcumin-chitosan mixture under continuous magnetic stirring at 1000 rpm at room temperature for 30 min. Nanoparticle formation proceeds immediately upon TPP addition due to the electrostatic crosslinking reaction between the protonated amino groups ($–NH_3^+$) of chitosan and the phosphate groups (PO_4^{3-}) of TPP. The resulting nanoparticle suspension was then allowed to rest undisturbed at room temperature for 1 hour to facilitate particle maturation and stabilization. When required by the experimental design, the solution pH was adjusted to 3.0, 4.0 or 5.0 prior to TPP addition using 0.1 M sodium hydroxide (NaOH) or 0.1 M hydrochloric acid (HCl).

A systematic one-factor-at-a-time (OFAT) approach was utilized to evaluate the influence of individual formulation parameters on nanoparticle formation and physicochemical properties. In each experimental set, only one parameter was varied while all remaining parameters were kept constant. The detailed experimental design and the specific values for each study variation are summarized in Table 1.

Table 1. Summary of OFAT experimental design for nanoparticle formulation parameters

Parameters	Level Tested	Fixed Parameters
Chitosan concentration (CS)	0.5, 1.0 and 1.5 mg/mL	TPP concentration (1.0 mg/mL, CS:TPP mass ratio (4:1), pH 5.0, curcumin loading (5% w/w)
TPP concentration	1.0, 10.0, 20.0 mg/mL	CS concentration (1.0 mg/mL, CS:TPP mass ratio (4:1), pH 5.0, curcumin loading (5% w/w)
CS:TPP mass ratio	3:1, 4:1, 5:1	CS concentration (1.0 mg/mL), TPP concentration (1.0 mg/mL), CS:TPP mass ratio (4:1), pH 5.0, curcumin loading (5% w/w)
Curcumin loading	5%, 10%, 20% w/w (relative to CS)	CS concentration (1.0 mg/mL), TPP concentration (1.0 mg/mL), CS:TPP mass ratio (4:1), pH 5.0,

Values represent the specific levels tested under the one-factor-at-a-time (OFAT) design; all other parameters within each respective study set were maintained constant.

2.3 Physicochemical characterization

2.3.1 Particle size and zeta potential analysis

The particle size and zeta potential of the prepared nanoparticles were determined using dynamic light scattering (DLS) with a Zetasizer Nano ZS90 (Malvern Instruments, UK). Nanoparticle suspensions were diluted 1:200 (v/v) in ultrapure water prior to measurement. The particle size was reported as the Z-average diameter, while the PDI provided a

measure of particle size distribution uniformity, with values ≤ 0.3 indicating a narrow, uniform distribution (Anand et al., 2007). Zeta potential measurements were conducted on filtered nanoparticle suspensions at 25°C using laser doppler electrophoresis. All measurements were performed in triplicate (n = 3) with at least three independent nanoparticle preparations to ensure reproducibility and statistical validity.

2.3.2 Nanoparticle tracking analysis (NTA)

Nanoparticle tracking analysis (NTA) was performed using a NanoSight NS300 instrument (Malvern Instruments, UK) equipped with a 488 nm laser and light scattering detection module as a complementary technique to DLS for real-time particle sizing and concentration determination. Optimized CRCSNP suspension was diluted 1:1000 (v/v) in ultrapure water. Video recordings of particle Brownian motion were captured for 30 s at 25°C with a frame rate of 24.97 fps and camera exposure of 40.00 ms using light scattering detection with contrast gain set to 2.00. Particle size distribution and number concentration were determined by automated particle tracking software (version 1.2.0.3, Build 20001013) through analysis of individual particle trajectories. All measurements were conducted in triplicate (n = 3) with at least three independent nanoparticle preparations to cross-validate the DLS results and assess particle size distribution and dispersion characteristics.

2.3.3 Fourier-transform infrared (FTIR) spectroscopy

FTIR spectroscopy was performed using a Perkin Elmer spectrometer (Perkin Elmer, USA) equipped with attenuated total reflectance (ATR) attachment. Measurements were conducted over a wavenumber range of 400-4000 cm^{-1} with a spectral resolution of 4 cm^{-1}, with each spectrum representing the average of 20 scans per sample. Analysis was conducted on raw chitosan, curcumin, sodium tripolyphosphate, a physical mixture of all three components, and the prepared CRCSNP formulation. This analysis was undertaken to identify intermolecular interactions between curcumin and chitosan through examination of characteristic absorption band shifts and to confirm the occurrence of ionic crosslinking between chitosan's amino groups and TPP's phosphate groups (Amalraj et al., 2017).

2.3.4 Encapsulation efficiency and loading efficiency of curcumin

Encapsulation efficiency (EE) and loading efficiency (LE) were determined by centrifugation and quantitative analysis. Aliquots of CRCSNP suspension (1 mL) were centrifuged at 10,000 × g for 30 min at 4°C using Amicon Ultra-15 Centrifugal Filter Units with Ultracel-10 membrane (MWCO = 10 kDa; Merck Millipore, Billerica, MA, USA). The supernatant, containing free (unentrapped) curcumin, was separated and analyzed for curcumin content by UV-Vis spectrophotometry at 425 nm. The nanoparticle pellet was then dissolved in 1 mL of methanol to release the encapsulated curcumin from the polymer matrix, and curcumin concentration was similarly determined. The encapsulation efficiency was calculated as equation 1:

$$\text{EE (\%)} = \left[\frac{(\text{Total curcumin - Free curcumin})}{\text{Total curcumin}}\right] \times 100 \quad (1)$$

While the loading efficiency was calculated as equation 2:

$$LE\ (\%) = \left[\frac{(\text{Total curcumin - Free curcumin})}{\text{Nanoparticle mass}}\right] \times 100 \quad (2)$$

2.4 Determination of curcumin solubility

Curcumin quantification was performed using UV-Vis spectrophotometry at a maximum wavelength (λ_{max}) of 425 nm. A stock solution (0.1 mg/mL) was prepared by dissolving 1.0 mg of curcumin in 10 mL of methanol. Serial dilutions were prepared in the concentration range of 1-5 µg/mL and analyzed at 425 nm to establish a linear standard curve. The resulting calibration curve ($y = 0.1465x - 0.0913$, $R^2 = 0.9992$) was employed for subsequent curcumin quantification.

Solubility studies were performed by incubating equal amounts (5 mg) of free curcumin and CRCSNsPs separately in 10 mL of six different test media under constant 37°C for 24 h. The dissolution media were prepared using 0.01 M phosphate buffer (pH 7.4), 0.01 M acetate buffer (pH 5.5 or pH 4.5), acetate buffer supplemented with 0.5% or 2.0% SLS, and acetate buffer supplemented with 0.1% or 1.0% Tween 20.

Sodium lauryl sulfate (SLS) and Tween 20 were included as representative anionic and non-ionic surfactants, respectively, to compare surfactant-assisted solubilization under different ionic conditions. The selected concentrations were intended to evaluate concentration-dependent effects on micellization, wetting, and curcumin solubilization. Tween 20 was chosen for its good aqueous compatibility, low toxicity, and established use in solubility and dissolution studies, whereas SLS was included as a representative anionic surfactant with strong solubilizing potential.

Following incubation, the suspensions were filtered through 0.45 µm cellulose acetate membrane filters, diluted as necessary, and the curcumin concentration was determined by UV-Vis spectrophotometry at 425 nm based on the established calibration curve. All experiments were conducted in triplicate (n = 3).

2.5 Statistical analysis

All data were presented as mean±standard deviation (SD). One-way analysis of variance (ANOVA) followed by post hoc Tukey's test was employed to assess statistical differences between treatment groups. Additionally, an independent-sample t-test was used to evaluate the significant differences in solubility between free curcumin and CRCSNPs within each respective dissolution medium, with $p<0.05$ considered statistically significant. GraphPad Prism 9.0 (San Diego, CA, USA) was used for all statistical analyses and graphical presentations.

3. Results and Discussion

3.1 Optimization of nanoparticle formation parameters

3.1.1 Effect of chitosan and TPP concentration

Chitosan and TPP concentrations are critical factors governing nanoparticle nucleation and colloidal stability (Dash et al., 2011; Ali & Ahmed, 2018). To evaluate the effect of chitosan concentration, chitosan was varied from 0.5 to 1.5 mg/mL while TPP concentration and formulation pH were kept constant. In a separate experiment, TPP concentration was varied from 1.0 to 20.0 mg/mL while chitosan concentration and formulation pH were fixed.

Significant variations in nanoparticle formation were observed under these conditions as shown in Figures 1A and 1B.

At 0.5 mg/mL chitosan, nanoparticles appeared to form initially, but visible precipitation was observed during the 1-h observation period. At 1.0 mg/mL, the nanoparticle suspension remained visually homogeneous over the same period. In contrast, increasing the chitosan concentration to 1.5 mg/mL resulted in the formation of large suspended aggregates and marked turbidity. The excessive polymer concentration (at chitosan concentration of 1.5 mg/mL) leads to network saturation and aggregation, which was consistent with previous reports on the chitosan/TPP system (Dash et al., 2011).

Similarly, varying the TPP concentration (1.0, 10.0, and 20.0 mg/mL) while maintaining chitosan at 1.0 mg/mL yielded comparable trends (Figure 1B). Stable nanoparticles were produced at TPP concentrations of 1.0 and 10.0 mg/mL, without precipitation after 1 h storage. However, at 20.0 mg/mL, the formation of large suspended aggregates resulted in complete light obstruction, indicating that excessive crosslinker induced macro-scale aggregation.

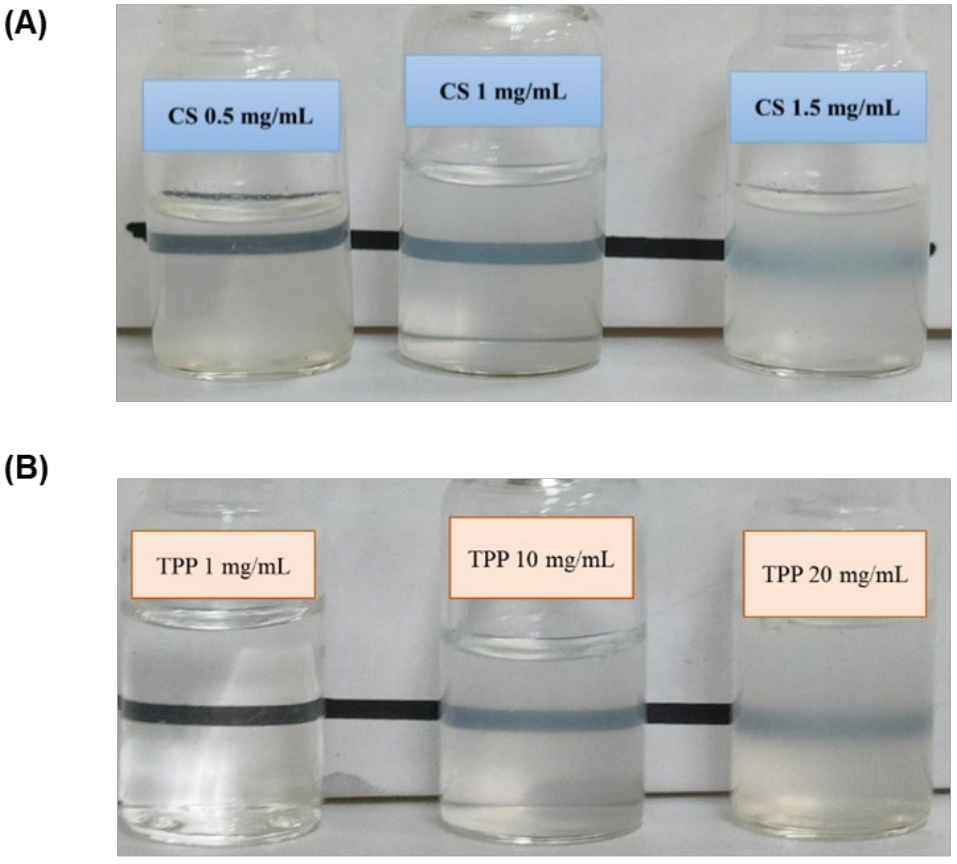

Figure 1. Influence of chitosan (A) and TPP (B) concentrations on nanoparticle characteristics. Visual assessment of blank chitosan nanoparticle (CSNP) suspensions after 1-h incubation at room temperature. Stable suspensions remained clear without visible precipitation or aggregation.

The ionic gelation mechanism requires a critical minimum threshold of amino groups ($-NH^{3+}$) on chitosan backbone to establish the electrostatic attraction with TPP phosphate groups ($-PO_4^{3-}$) necessary for stable ionic crosslinks (Dash et al., 2011). At low chitosan concentration (≤ 0.5 mg/mL), the lack of cationic charge density prevents a solid ionic network forming, resulting in particle instability and precipitation. Conversely, an excess of TPP increases the ionic strength of the solution, which neutralizes the electrostatic repulsion between polymer chains, leading to aggregation and precipitation (Dash et al., 2011).

The optimal concentration range (chitosan: 1.0 mg/mL, TPP: 1.0-10.0 mg/mL) represents the balance between charge availability and osmotic stability of the dispersed phase. In all formulations, the stirring speed was kept constant at 1000 rpm to minimize hydrodynamic variability; under these conditions, the observed changes in particle size and colloidal stability were attributed primarily to the CS:TPP ratio, pH, and curcumin loading rather than to differences in stirring kinetics.

3.1.2 Effect of CS:TPP mass ratio

The effect of the chitosan-to-TPP mass ratio on nanoparticle characteristics was investigated by varying the ratio from 3:1 to 5:1, while maintaining the formulation pH at 5.0 and fixing the curcumin loading at 5% w/w relative to chitosan. Under these conditions, substantial differences in the characteristics of both blank chitosan nanoparticles (CSNP) and curcumin loaded chitosan nanoparticles (CRCSNP) were observed as shown in Table 2. For CSNP, the 4:1 ratio produced particles with the smallest diameter (106.3±1.5 nm) and lowest polydispersity (0.217±0.035), indicating optimal crosslinking density and uniform particle formation. The 3:1 ratio produced slightly larger particles (112.6±1.5 nm), while the 5:1 ratio produced particles of similar size (111.3±2.7 nm).

Table 2. Influence of cs:tpp mass ratio on the physicochemical characteristics of curcumin-loaded chitosan nanoparticles (pH 5.0, 5% w/w curcumin loading)

CS: TPP Ratio	Size (nm)		Zeta Potential (mV)		EE (%)
	CSNP	CRCSNP	CSNP	CRCSNP	CRCSNP
3:1	112.6±1.5^{a}	269.6±24.2^{b}	26.33±1.01^{b}	19.59±1.21^{b}	74.04±0.75^{c}
4:1	106.3±1.5^{b}	211.9±10.6^{c}	29.88±0.71^{a}	21.54±1.17^{ab}	96.88±0.06^{a}
5:1	111.3±2.7^{a}	324.7±7.4^{a}	27.39±1.34^{b}	22.66±0.83^{a}	84.36±0.52^{b}

Values are expressed as mean±SD (n = 3). Different superscript letters within the same column indicate statistically significant differences among CS:TPP mass ratios (one-way ANOVA followed by Tukey's HSD test, $p<0.05$). CRCSNP formulations were prepared at pH 5.0 with 5% w/w curcumin loading relative to chitosan.

When curcumin was incorporated at 5% loading (Table 2), the 4:1 ratio also demonstrated superior characteristics, producing the smallest CRCSNPs (211.9±10.6 nm) with good size uniformity and the highest zeta potential (21.54±1.17 mV), indicating maximum surface charge density. In contrast, the 3:1 ratio resulted in considerably larger particles (269.6±24.2 nm) with lower zeta potential (19.59±1.21 mV), suggesting incomplete crosslinking. For the 5:1 ratio, the CRCSNPs exhibited a further size increase

(324.7±7.4 nm) with reduced uniformity, while encapsulation efficiency continued to increase slightly (74.0% at 3:1 ratio, 81.7% at 4:1, 84.3% at 5:1 ratio).

The optimal 4:1 mass ratio represented an optimal balance between multiple competing factors. At lower ratios (3:1), the low ionic crosslinking density prevented a complete polymer network formation, resulting in larger particles with a broad size distribution and poor drug encapsulation. Conversely, at higher ratios (5:1), the excess of chitosan—despite providing more amino groups—lead to uncontrolled aggregation and increased particle size. The 4:1 ratio resulted in an optimal level of crosslinking, which was reflected in the low PDI and high charge density. This produces tightly-packed nanoparticles that maintained high colloidal stability (Dash et al., 2011).

3.1.3 Effect of pH

The pH of a solution is a fundamental parameter controlling the ionization of chitosan's amino groups, which directly impact the electrostatic interactions essential for ionic gelation (Mao et al., 2004). The effect of pH on nanoparticles formation was evaluated at pH 3.0, 4.0 and 5.0 using formulations containing 5% w/w curcumin relative to chitosan and fixed CS:TPP ratio mass ratio of 4:1. In this experiment, only the formulation pH was varied, whereas both the CS:TPP mass ratio and curcumin loading were kept constant. As pH increased from 3.0 to 5.0, dramatic changes in particle size, zeta potential and encapsulation efficiency were observed, as shown in Table 3. At pH 3.0, CSNPs exhibited a diameter of 143.5±3.1 nm with relatively low zeta potential (19.21±0.36 mV) and CRCSNPs had size of 161.2±3.2 nm with low encapsulation efficiency (57.84±0.68%). As pH increased to 4.0, the CSNP size remained similar (141.8±12.0 nm) but zeta potential increased to 24.86±1.54 mV. Further increase to pH 5.0 produced the smallest blank CSNPs (106.3±1.5 nm) with the highest zeta potential (29.88±0.71 mV). For CRCSNP, pH 5.0 achieved the largest particle size (211.9±10.6 nm) but with optimal encapsulation efficiency (96.88±0.06%), representing a 3.0 percentage point increase from pH 3.0 ($p<0.05$).

Table 3. Influence of pH on the physicochemical characteristics of curcumin-loaded chitosan nanoparticles (cs:tpp 4:1, 5% w/w curcumin loading)

pH	Size (nm)		Zeta Potential (mV)		EE (%)
	CSNP	CRCSNP	CSNP	CRCSNP	
3.0	143.5±3.1^{a}	161.2±3.2^{c}	19.21±0.36^{b}	14.83±2.03^{b}	57.84±0.68^{b}
4.0	141.8±12.0^{a}	180.1±20.7^{b}	24.86±1.54^{ab}	21.19±0.55^{a}	60.47±0.64^{b}
5.0	106.3±1.5^{b}	211.9±10.6^{a}	29.88±0.71^{a}	21.54±1.17^{a}	96.88±0.06^{a}

Values are expressed as mean ± SD (n = 3). Different superscript letters within the same column indicate statistically significant differences among pH values (one-way ANOVA followed by Tukey's HSD test, $p<0.05$). The CS:TPP mass ratio was fixed at 4:1 and curcumin loading was fixed at 5% w/w relative to chitosan.

The pH-dependent effects reflect two simultaneous mechanisms affecting nanoparticle formation. Primarily, pH controls the degree of protonation of chitosan's amino groups, which have a pK_a of approximately 6.5. At pH 3.0, excess hydronium ions (H^+) compete with TPP phosphate groups for binding to amino groups. This competition limits the availability of $-NH_3^+$ groups for effective ionic crosslinking, leading to the destabilization of the developing polymer network. As the pH increases to pH 5.0, remaining below the

pK_a of chitosan, an optimal protonation level is reached. This enhances the electrostatic attraction between the polymer and the crosslinker, resulting in a densely crosslinked network with enhanced colloidal stability. (Mao et al., 2004; Gan et al., 2005)

Furthermore, pH significantly influences the physicochemical properties of both curcumin and the nanoparticle matrix. Curcumin remains chemically stable but poorly soluble in acidic conditions; however, it can be effectively loaded into nanoparticles using a pH-driven approach (Pan et al., 2013). While curcumin's phenolic hydroxyl groups have pK_a values between 7.5 and 8.5, its encapsulation at pH 5.0 is primarily driven by the optimal protonation of the carrier matrix, such as chitosan ($pK_a \approx 6.5$) (Pan et al., 2013; Li et al., 2024). At this pH, the strong electrostatic interactions and the formation of a robust polymer network led to a high encapsulation efficiency of 80.8% (Table 2). This observation is consistent with the findings of Li et al. (2024), as these ionic interactions are essential for high drug entrapment in chitosan systems (Li et al., 2024). Moreover, this acidic environment ensures that the nanoparticles maintain a high positive zeta potential, preventing particle aggregation and ensuring a suitable particle size for effective oral absorption (Chuah et al., 2014).

3.1.4 Effect of curcumin loading

Curcumin loading significantly influenced the physicochemical properties of the nanoparticles, reflecting the limited carrying capacity of the chitosan-TPP matrix. To evaluate this effect, curcumin loading varied from 5% to 20% w/w relative to chitosan while the formulation pH and CS:TPP mass ratio were fixed at 5.0 and 4:1, respectively. Under these optimized conditions, systematic changes in particle size, surface charge, and encapsulation efficiency were observed (Table 4). Blank CSNPs exhibited a mean diameter of 106.3±1.5 nm with a zeta potential of 29.88±0.71 mV. Upon incorporation of 5% curcumin, the particle size increased to 211.9±10.6 nm and the zeta potential decreased to 21.54±1.17 mV, while the encapsulation efficiency remained high at 96.88±0.06%. Increasing the curcumin loading to 10% and 20% led to further particle enlargement and a progressive decline in zeta potential, accompanied by marked reductions in encapsulation efficiency. Specifically, particle size increased to 262.9±1.2 nm and 264.7±11.0 nm, zeta potential decreased to 10.34±0.95 mV and 7.51±0.72 mV, and encapsulation efficiency declined to 70.56±1.84% and 50.61±0.51%, respectively.

The inverse relationship between curcumin loading and charge density revealed competing interactions within the nanoparticle matrix. At low loading (5%), curcumin is effectively incorporated through both hydrophobic partitioning into the polymer matrix and hydrogen bonding between its phenolic hydroxyl and carbonyl groups and chitosan's protonated amino groups ($-NH_3^+$), resulting in high encapsulation efficiency (Fan et al., 2012). However, curcumin loading beyond 5% exceeded the molecular carrying capacity of the chitosan-TPP matrix, leading to several interfacial changes. Curcumin molecules compete for $-NH_3^+$ sites on chitosan, reducing the number of free positive charges available for electrostatic stabilization. This effect was evidenced by the decrease in zeta potential from +16.35 mV at 5% to +7.51 mV at 20% loading. Furthermore, excess curcumin interferes with ionic crosslinking between chitosan and TPP by competing for protonated amino group interactions, which weakens the polymer network structure and reduces its mechanical integrity (Chuah et al., 2014). Beyond the matrix saturation point, this excess curcumin presumably precipitates or crystallizes, accumulating at particle surface or exterior. This phenomenon explains the substantial loss in encapsulation efficiency from 96.88% at 5% to 50.61% at 20%. The combined effect of a weakened network and surface-

bound curcumin molecules contributes to particle enlargement and increased size heterogeneity, explaining the rise in both particle size and polydispersity index.

Table 4. Influence of curcumin loading on the physicochemical characteristics of curcumin-loaded chitosan nanoparticles (cs:tpp 4:1, pH 5.0)

Curcumin (%)	Size (nm)	Zeta Potential (mV)	Entrapment Efficiency (%)	Loading Efficiency (%)
0	106.3±1.5^{c}	29.88± 0.71^{a}	-	-
5	211.9±10.6^{b}	21.54±1.17^{b}	96.88±0.06^{a}	4.61±0.00^{b}
10	262.9±1.2^{a}	10.34±0.95^{c}	70.56±1.84^{b}	6.41±0.17^{a}
20	264.7±11.0^{a}	7.51±0.72^{c}	50.61±0.51^{c}	6.60±0.17^{a}

Values are expressed as mean±SD (n = 3). Different superscript letters within the same column indicate statistically significant differences among curcumin loadings (one-way ANOVA followed by Tukey's HSD test, $p<0.05$). Formulations were prepared at pH 5.0 using a fixed CS:TPP mass ratio of 4:1.

The results show that 5% curcumin loading is the optimal point for obtaining both high drug encapsulation and colloidal stability. This finding is essential for rational formulation design and scale-up manufacturing of CRCSNP products.

In this study, a single low-molecular-weight chitosan was employed to isolate the effects of CS:TPP ratio, pH, and curcumin loading; and therefore, the impact of chitosan molecular weight on encapsulation efficiency therefore remains to be explored in future formulations.

At the optimized curcumin loading of 5% w/w, CRCSNP achieved an encapsulation efficiency of 96.9%, which is higher than or comparable to the values reported for curcumin-loaded chitosan nanoparticles prepared by ionic gelation and related methods, where encapsulation efficiencies in the range of approximately 70-90% were described for wound healing, antimicrobial, and antifibrotic applications (Kumbhar et al., 2023; Aguilera et al., 2025; Hasanzade et al., 2025).

3.2 Nanoparticle tracking analysis (NTA)

Nanoparticle tracking analysis (NTA) was used as a complementary technique to dynamic light scattering (DLS) to provide single-particle size distribution and particle concentration for the optimized CRCSNP formulation. In contrast to DLS, which reports an intensity-weighted hydrodynamic diameter, NTA tracks individual particle Brownian motion and therefore provides number-based size distribution information and absolute particle concentration. The optimization formulation exhibited a mode diameter of 162.5 nm and a mean size of 230 nm, with D10, D50, and D90 values of 92 nm, 189 nm, and 400 nm, respectively. The particle size distribution and particle concentration data obtained by NTA are clearly illustrated in Figure 2, which shows a measured particle concentration of 2.76×10^{11} particles/mL, which correlates with the DLS-derived PDI of 0.351, indicating a well-dispersed nanoparticle population. Furthermore, the zeta potential of +21.54±1.17 mV indicates moderate electrostatic stabilization. Although this value is below the ±30 mV threshold for long-term stability, the positive surface charge provides sufficient repulsion to prevent immediate aggregation in aqueous suspension. The formation of CSNP and

CRCSNP was confirmed through particle concentration measurement and individual particle Brownian motion tracking by NTA. This corresponds to the reported characterization of curcumin-loaded chitosan nanoparticles, where Chuah et al. (2014) showed that NTA offers better size distribution and particle count accuracy than conventional dynamic light scattering. The NTA results in our studies were consistent with the DLS-derived size trend and supported the conclusion that the optimized CRCSNP formulation was colloidally stable and predominantly within the nanoscale range. The comprehensive dataset of the NTA parameters, including the mode, mean, and specific percentile values, is summarized in Table 5. These results indicate a well -dispersed nanoparticle population in our optimized CRCSNP formulation at the time of measurement.

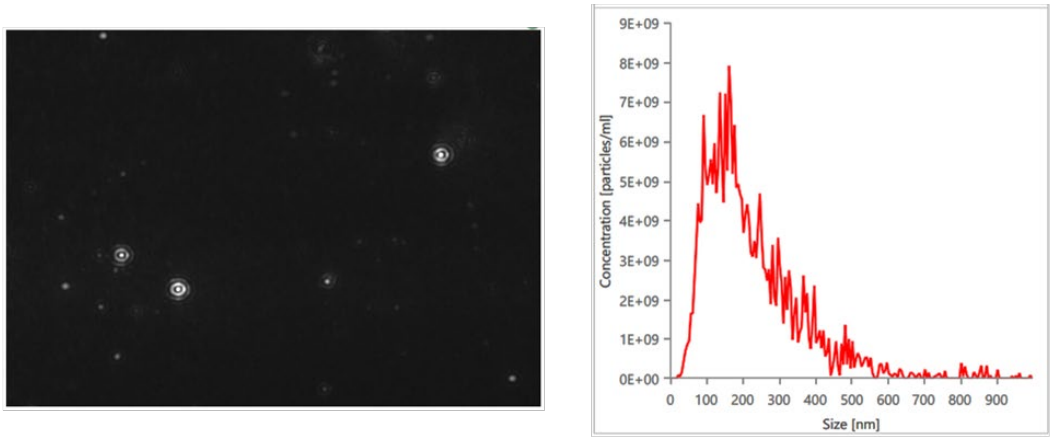

Figure 2. Nanoparticle tracking analysis of CRCSNPs. (A) Representative field image showing individual CRCSNP particles undergoing Brownian motion. (B) Number-based size distribution histogram obtained by NTA, illustrating the distribution of particle diameters and the corresponding particle concentration. NTA was used as a complementary method to DLS to verify the presence of a narrow nanoscale population and to determine particle concentration

Table 5. Particle size distribution and concentration of optimized curcumin-loaded chitosan nanoparticles (CRCSNPs) determined by nanoparticle tracking analysis (nta) (CS:TPP 4:1, pH 5.0, 5% w/w curcumin loading)

Parameters	Values
Mode [nm]	162.5
Mean [nm]	230
Standard deviation [nm]	151
Concentration [particles/ml]	2.76×10^{11}
D10 [nm]	92
D50 [nm]	189
D90 [nm]	400

3.3 FTIR spectroscopy

Fourier-transform infrared spectroscopy was employed to analyze molecular interactions, providing evidence for the ionic gelation process and successful drug encapsulation (Figure 3). The spectrum of raw chitosan revealed characteristic O-H and N-H stretching vibrations at 3460 cm^{-1}, aliphatic C-H stretching at 2885 cm^{-1}, amide I band (acetyl C=O) at 1656 cm^{-1}, amide II band (free amino N-H) at 1575 cm^{-1}, and glycosidic C-O-C stretching at 1063 cm^{-1} (Fan et al., 2012). Pure curcumin exhibited O-H stretching from phenolic groups at 3500 cm^{-1}, aromatic C=C and keto-enol C=O vibrations at 1606 and 1508 cm^{-1}, and phenolic C-O stretching at 1256 cm^{-1} (Anitha et al., 2012). Sodium tripolyphosphate showed asymmetric P=O stretching vibrations at 1134 and 910 cm^{-1} characteristic of phosphate functional groups (Dudhani & Kosaraju, 2010).

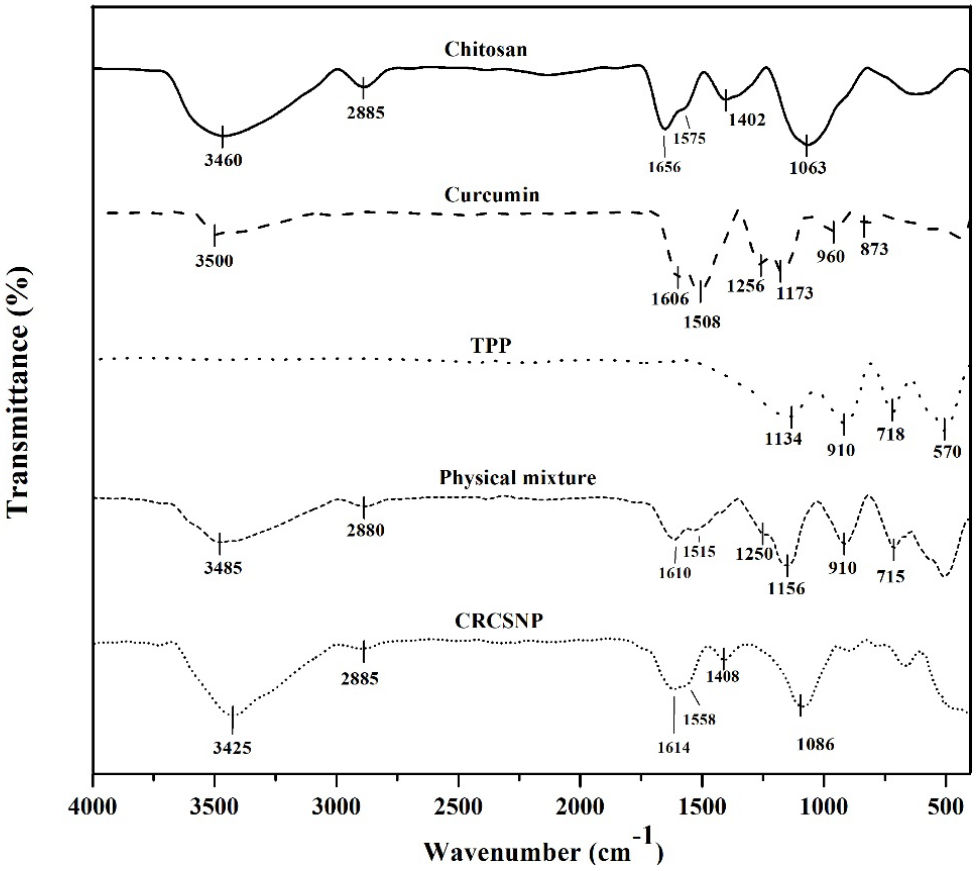

Figure 3. FTIR spectra of curcumin-loaded chitosan nanoparticles (CRCSNPs). The spectra shown are those of raw materials (chitosan, curcumin, sodium tripolyphosphate), physical mixture, and optimized CRCSNP formulation (CS:TPP 4:1, pH 5.0, 5% w/w curcumin loading). Peak shifts indicate ionic crosslinking and molecular interactions between components.

In the physical mixture of chitosan, curcumin, and TPP, individual spectral peaks remained separate and unchanged, showing only a simple blending without chemical interaction. In contrast, the FTIR spectrum of the optimized CRCSNPs showed several peak shifts and changes, as shown in Figure 3. These peak shifts and changes provide evidence of the formation of nanoparticles. The O–H and N–H stretching band of chitosan appeared at 3460 cm^{-1}, whereas in the physical mixture this band shifted slightly to 3485 cm^{-1} and in CRCSNPs, the peak is shifted to a broader band centered around 3425 cm^{-1}, consistent with enhanced hydrogen bonding between chitosan, TPP, and curcumin (Fan et al., 2012). This peak shift to a higher wavenumber or broadening is a classic indicator of the complexation between the polymer matrix and curcumin (Anitha et al., 2012).

More significantly, the amide I and amide II bands, which serve as indicators of chitosan's amino group protonation, shifted during the process. The amide I band moved from 1656 cm^{-1} to 1614 cm^{-1}, while the amide II band changed from 1575 cm^{-1} to 1558 cm^{-1}. These lower frequency shifts show the protonation of amino groups ($-NH_2 \rightarrow -NH_3^+$) and the formation of ionic interactions between the positively charged protonated amino groups and negatively charged phosphate groups (PO_4^{3-}) of TPP (Akhtar et al., 2012; Fan et al., 2012). This evidence confirms that ionic crosslinking is the main mechanism for nanoparticle formation. Hydrogen bonding between curcumin's functional groups and chitosan further stabilizes the structure and increases curcumin retention within the matrix. The weakening of curcumin's characteristic peaks at 1606, 1508, and 1256 cm^{-1} in the CRCSNP spectrum suggests that the bioactive compound was incorporated within the nanoparticle matrix rather than surface-adsorbed (Akhtar et al., 2012; Anitha et al., 2012). This is important for ensuring sustained release and protection from degradation. It should be noted, however, that peak overlap with chitosan and TPP absorption bands may also contribute to the reduced intensity; therefore, this reduction is interpreted as evidence of strong curcumin–polymer interactions and matrix encapsulation.

3.4 Curcumin solubility

Solubility studies revealed that CRCSNP successfully enhanced curcumin solubility across all tested media, ranging from 1.3-fold to 2.0-fold higher than free curcumin (Table 6). In 0.01 M phosphate buffer at pH 7.4 (physiological pH), free curcumin showed a solubility of 1.46±0.04 µg/mL, while CRCSNP reached 2.83±0.06 µg/mL, representing a modest 1.3-fold increase. In contrast, in 0.01 M acetate buffer at pH 4.5 (mimicking the mildly acidic conditions of the gastrointestinal tract), free curcumin exhibited its lowest solubility at 2.24±0.03 µg/mL, whereas CRCSNP reached 4.19±0.06 µg/mL. This 2.0-fold increase demonstrates that the nanoparticles significantly improve solubility in weakly acidic environments.

The addition of surfactants to simulate the fed state or enhance gastrointestinal absorption increased the solubility of both free curcumin and CRCSNP, which can be attributed to micellization and emulsification. In acetate buffer (pH 4.5) with 0.5% SLS (Table 6), free curcumin solubility rose to 8.98±0.24 µg/mL, while CRCSNP reached 14.54±0.10 µg/mL, corresponding to a 1.6-fold enhancement. At 2% SLS, solubility further increased to 11.88±0.68 µg/mL for free curcumin and 18.76±0.22 µg/mL for CRCSNP, corresponding to a 1.5-fold enhancement. Tween 20 showed a similar trend: at 0.1% concentration, free curcumin solubility was 6.40±0.03 µg/mL, compared with 17.46±0.33 µg/mL for CRCSNP, representing a 2.8-fold enhancement, while at 1% Tween 20, the values were 17.09±0.23 µg/mL and 22.60±0.17 µg/mL, respectively, corresponding to a

1.3-fold enhancement. Overall, both SLS and Tween 20 enhanced curcumin solubility, with the effect depending on surfactant type and concentration.

The solubility enhancement of CRCSNP arises from several integrated mechanisms. The peak performance at pH 4.5 correlates with the protonation of chitosan's amino groups. This creates a charged, hydrophilic surface that stabilizes encapsulated curcumin and promotes dissolution through electrostatic shielding and hydration layer formation (Akhtar et al., 2012; Duse et al., 2018). Additionally, the hydrophilic polysaccharide shell, rich in hydroxyl and amino groups, improves wetting and reduces interfacial tension, facilitating better aqueous contact and increasing the apparent solubility of the encapsulated curcumin (Anitha et al., 2012).

Table 6. Comparative solubility of free curcumin and optimized curcumin-loaded nanoparticles (CRCSNP) in different dissolution media (CS:TPP 4:1, pH 5.0, 5% w/w curcumin loading)

Dissolution Media	Solubility of Curcumin (µg/mL)	
	Free Curcumin	CRCSNPs
phosphate buffer pH 7.4	1.46±0.04^{f}	2.83±0.06$^{g,\ *}$
acetate buffer pH 6.5	1.38±0.03^{f}	3.74±0.09$^{fg,\ *}$
acetate buffer pH 4.5	2.24±0.03^{ef}	4.19±0.06$^{f,\ *}$
acetate buffer pH 4.5 + 0.1% Tween20	6.40±0.03^{d}	17.46±0.33$^{bc,\ *}$
acetate buffer pH 4.5 + 1% Tween20	17.09±0.23^{a}	22.60±0.17$^{a,\ *}$
acetate buffer pH 6.5 + 0.1% Tween20	6.87±0.07^{d}	16.17±0.26$^{cd,\ *}$
acetate buffer pH 6.5 + 1% Tween20	15.20±0.38^{b}	18.93±0.10$^{b,\ *}$
phosphate buffer pH 7.4 + 0.1% Tween20	6.73±0.09^{d}	15.50±0.22$^{de,\ *}$
phosphate buffer pH 7.4 + 1% Tween20	15.33±0.33^{b}	17.88±0.27$^{bc,\ *}$
acetate buffer pH 4.5 + SLS 0.5%	8.98±0.24^{c}	14.54±0.10$^{e,\ *}$
acetate buffer pH 4.5 + SLS 2%	11.88±0.68^{b}	18.76±0.22$^{b,\ *}$

Results are shown as mean±SD of three independent experiments, n = 3. Different superscript letters within the same column indicate statistically significant differences among dissolution media (one-way ANOVA followed by Tukey's HSD test, $p<0.05$). The arterisk (*) indicates a statistically significant difference between Free curcumin and CRCSNPs within the same dissolution medium ($p<0.05$) using an independent-sample t-test.

The physical state of curcumin within the nanoparticles also plays a role in these results. FTIR analysis showed that curcumin's characteristic peaks became less sharp and intense, suggesting molecular dispersion within the chitosan matrix. While some overlap with polymer bands may occur, this change in physical form is a key factor behind the increased solubility compared to the original crystalline form of curcumin (Akhtar et al., 2012; Anitha et al., 2012). This integration is stabilized by hydrogen bonding between the phenolic hydroxyl (-OH) and carbonyl (C=O) groups of curcumin and the protonated amino

groups (-NH3+) of chitosan. These interactions effectively prevent drug aggregation and recrystallization, thereby maintaining enhanced solubility throughout the dissolution process (Anitha et al., 2012).

The addition of surfactants (SLS or Tween 20) increased the solubility of both free curcumin and CRCSNP through micellization and emulsification. Under these conditions, CRCSNP yielded higher curcumin concentrations than the free drug, indicating that chitosan's electrostatic stabilization synergizes with surfactant-mediated solubilization (Duse et al., 2018). This interaction suggests that administering CRCSNP with dietary fats (which induce endogenous surfactant secretion) or pharmaceutical surfactants may enhance bioavailability beyond that of free curcumin (Akhtar et al., 2012; Duse et al., 2018).

The solubility enhancement observed in this study (up to 2.8-fold) is modest compared to more complex nanoformulation systems reported in the literature. While an improvement over free curcumin is achieved, more sophisticated delivery systems have demonstrated substantially higher solubility increases (Guzman-Villanueva et al., 2013). However, the current results are comparable to other chitosan-based ionotropic gelation systems and suggest that the approach provides a foundation for further optimization.

4. Conclusions

This study successfully optimized curcumin-loaded chitosan nanoparticles prepared by ionic gelation using a chitosan-to-TPP ratio of 4:1 at pH 5.0 with 5% curcumin loading. The resulting nanoparticles exhibited uniform size distribution, high encapsulation efficiency, and FTIR spectra indicating ionic crosslinking between chitosan and TPP. Solubility was substantially enhanced in acetate buffer (pH 4.5) and was further improved in the presence of Tween 20 compared with free curcumin. Overall, the findings indicate that the enhancement of curcumin solubility results from the combined effects of chitosan protonation, TPP-mediated ionic crosslinking, and curcumin–chitosan interactions, which together modulate nanoparticle structure, surface charge, and dispersibility. These mechanistic insights provide formulation guidance for extending chitosan-based nanocarriers to other poorly water-soluble bioactive compounds. The use of design of experiments (DoE) methodologies is recognized as a potential pathway for future optimization as it allows for a more detailed refinement of the formulation by examining interaction effects between variables.

5. Acknowledgements

The authors gratefully acknowledge the Faculty of Pharmacy, Srinakharinwirot University, for providing the research facilities and analytical instrumentation necessary for this study. Special thanks are extended to the laboratory and technical staff for their assistance with nanoparticle characterization and HPLC analysis. This work was supported by research funding from the Faculty of Pharmacy, Srinakharinwirot University, which enabled the systematic optimization and evaluation of curcumin-loaded chitosan nanoparticles.

6. Authors' Contributions

Chayut Fongsuk designed and performed the research, analyzed data, and drafted the manuscript; Chutwadee Krisanapun contributed to data analysis and manuscript preparation; and Duangratana Shuwisitkul supervised the study and finalized the manuscript.

ORCID
Duangratana Shuwisitkul https://orcid.org/0000-0002-5453-7503

7. Conflicts of Interest

The authors declare that they have no known competing financial interests or personal relationships that could have appeared to influence the work reported in this paper. This research was independently conducted using facilities and funding provided solely by the Faculty of Pharmacy, Srinakharinwirot University, with no involvement from commercial entities or external organizations in the study design, data collection, or interpretation of results.

8. AI Declaration

No AI Declaration is required as AI was used.

References

Aguilera, L. F., Araujo, L. O., Facchinatto, W. M., Lima, R. G., Pontes, M. D. S., Pulcherio, J. H. V., Caires, C. S. A., de Oliveira, K. T., de Oliveira, S. L., & Caires, A. R. L. (2025). Blue-light photoactivated curcumin-loaded chitosan nanoparticles prepared by nanoprecipitation and ionic gelation: A promising approach for antimicrobial photodynamic inactivation. *ACS Applied Bio Materials*, *8*(5), 4055-4064. https://doi.org/10.1021/acsabm.5c00200

Ahsan, S. M., Thomas, M., Reddy, K. K., Sooraparaju, S. G., Asthana, A., & Bhatnagar, I. (2018). Chitosan as biomaterial in drug delivery and tissue engineering. *International Journal of Biological Macromolecules*, *110*, 97-109. https://doi.org/10.1016/j.ijbiomac.2017.08.140

Akhtar, F., Rizvi, M. M. A., & Kar, S. K. (2012). Oral delivery of curcumin bound to chitosan nanoparticles cured *Plasmodium yoelii*-infected mice. *Biotechnology Advances*, *30*(1), 310-320. https://doi.org/10.1016/j.biotechadv.2011.05.009

Ali, A., & Ahmed, S. (2018). A review on chitosan and its nanocomposites in drug delivery. *International Journal of Biological Macromolecules*, *109*, 273-286. https://doi.org/10.1016/j.ijbiomac.2017.12.078

Amalraj, A., Pius, A., Gopi, S., & Gopi, S. (2017). Biological activities of curcuminoids, other biomolecules from turmeric and their derivatives - A review. *Journal of Traditional and Complementary Medicine*, *7*(2), 205-233. https://doi.org/10.1016/j.jtcme.2016.05.005

Anand, P., Kunnumakkara, A. B., Newman, R. A., & Aggarwal, B. B. (2007). Bioavailability of curcumin: problems and promises. *Molecular Pharmaceutics*, *4*(6), 807-818. https://doi.org/10.1021/mp700113r

Anitha, A., Maya, S., Deepa, N., Chennazhi, K. P., Nair, S. V., & Jayakumar, R. (2012). Curcumin-loaded N,O-carboxymethyl chitosan nanoparticles for cancer drug delivery. *Journal of Biomaterials Science, Polymer Edition*, *23*(11), 1381-1400 https://doi.org/10.1163/092050611x581534

Bockuviene, A., & Sereikaite, J. (2020). New β-carotene-chitooligosaccharides complexes for food fortification: Stability study. *Foods*, *9*(6), Article 765. https://doi.org/10.3390/foods9060765

Chuah, L. H., Roberts, C. J., Billa, N., Abdullah, S., Rosli, R., & Manickam, S. (2014). Using Nanoparticle tracking analysis (NTA) to decipher mucoadhesion propensity of curcumin-

containing chitosan nanoparticles and curcumin release. *Journal of Dispersion Science and Technology*, *35*(9), 1201-1207. https://doi.org/10.1080/01932691.2013.800458

Dash, M., Chiellini, F., Ottenbrite, R. M., & Chiellini, E. (2011). Chitosan—A versatile semi-synthetic polymer in biomedical applications. *Progress in Polymer Science*, *36*(8), 981-1014. https://doi.org/10.1016/j.progpolymsci.2011.02.001

Dudhani, A. R., Kosaraju, S. L. (2010). Bioadhesive chitosan nanoparticles: Preparation and characterization. *Carbohydrate Polymers*, *81*(2), 243-251. https://doi.org/10.1016/j.carbpol.2010.02.026

Duse, L., Baghdan, E., Pinnapireddy, S. R., Engelhardt, K. H., Jedelská, J., Schaefer, J., Quendt, P., & Bakowsky, U. (2018). Preparation and Characterization of Curcumin Loaded Chitosan Nanoparticles for Photodynamic Therapy. *Physica status solidi A*, *215*(15), Article 1700709. https://doi.org/https://doi.org/10.1002/pssa.201700709

Fan, W., Yan, W., Xu, Z., & Ni, H. (2012). Formation mechanism of monodisperse, low molecular weight chitosan nanoparticles by ionic gelation technique. *Colloids and Surfaces B: Biointerfaces*, *90*, 21-27. https://doi.org/10.1016/j.colsurfb.2011.09.042

Gan, Q., Wang, T., Cochrane, C., & McCarron, P. (2005). Modulation of surface charge, particle size and morphological properties of chitosan-TPP nanoparticles intended for gene delivery. *Colloids and Surfaces B: Biointerfaces*, *44*(2-3), 65-73. https://doi.org/10.1016/j.colsurfb.2005.06.001

Gera, M., Sharma, N., Ghosh, M., Huynh, D. L., Lee, S. J., Min, T., Kwon, T., & Jeong, D. K. (2017). Nanoformulations of curcumin: an emerging paradigm for improved remedial application. *Oncotarget*, *8*(39), 66680-66698. https://doi.org/10.18632/oncotarget.19164

Granata, G., Stracquadanio, S., Leonardi, M., Napoli, E., Malandrino, G., Cafiso, V., Stefani, S., & Geraci, C. (2021). Oregano and thyme essential oils encapsulated in chitosan nanoparticles as effective antimicrobial agents against foodborne pathogens. *Molecules*, *26*(13), Article 4055. https://doi.org/10.3390/molecules26134055

Guzman-Villanueva, D., El-Sherbiny, I. M., Herrera-Ruiz, D., & Smyth, H. D. (2013). Design and in vitro evaluation of a new nano-microparticulate system for enhanced aqueous-phase solubility of curcumin. *BioMed Research International*, *2013*, Article 724763. https://doi.org/10.1155/2013/724763

Hasanzade, P., Mosayebi, G., Ganji, A., Fahimirad, S., & Ghazavi, A. (2025). Curcumin-loaded chitosan nanoparticles: a promising approach to liver fibrosis prevention. *BMC Pharmacology and Toxicology*, *26*(1), Article 190. https://doi.org/10.1186/s40360-025-01031-w

Hewlings, S. J., & Kalman, D. S. (2017). Curcumin: A review of its effects on human health. *Foods*, *6*(10), Article 92. https://doi.org/10.3390/foods6100092

Kumbhar, S., Khairate, R., Bhatia, M., Choudhari, P., & Gaikwad, V. (2023). Evaluation of curcumin-loaded chitosan nanoparticles for wound healing activity. *ADMET & DMPK*, *11*(4), 601-613. https://doi.org/10.5599/admet.1897

Kowalczyk, A., Twarowski, B., Fecka, I., Tuberoso, C. I. G., & Jerković, I. (2024). Thymol as a component of chitosan systems—Several new applications in medicine: A comprehensive review. *Plants*, *13*(3), Article 362. https://doi.org/10.3390/plants13030362

Li, H., Zhao, M., Li, J., Wang, J., Zhang, H., Wang, J., Xia, N., Wang, Z., & Rayan, A. M. (2024). Advancing the pH-driven encapsulation technique of curcumin: Molecular interaction shifts due to structural and charge variations. *Food Hydrocolloids*, *152*, Article 109952. https://doi.org/10.1016/j.foodhyd.2024.109952

Mao, S., Shuai, X., Unger, F., Simon, M., Bi, D., & Kissel, T. (2004). The depolymerization of chitosan: effects on physicochemical and biological properties. *International Journal of Pharmaceutics*, *281*(1-2), 45-54. https://doi.org/10.1016/j.ijpharm.2004.05.019

Pan, K., Zhong, Q., & Baek, S. J. (2013). Enhanced dispersibility and bioactivity of curcumin by encapsulation in casein nanocapsules. *Journal of Agricultural and Food Chemistry*, *61*(25), 6036-6043. https://doi.org/10.1021/jf400752a

Sogias, I. A., Williams, A. C., & Khutoryanskiy, V. V. (2008). Why is chitosan mucoadhesive? *Biomacromolecules*, *9*(7), 1837-1842. https://doi.org/10.1021/bm800276d

Tan, Q., Liu, W., Guo, C., & Zhai, G. (2011). Preparation and evaluation of quercetin-loaded lecithin-chitosan nanoparticles for topical delivery. *International Journal of Nanomedicine*, *6*, 1621-1630. https://doi.org/10.2147/IJN.S22411

Urošević, M., Nikolić, L., Gajić, I., Nikolić, V., Dinić, A., & Miljković, V. (2022). Curcumin: Biological activities and modern pharmaceutical forms. *Antibiotics*, *11*(2), Article 135. https://doi.org/10.3390/antibiotics11020135

Walbi, I. A., Ahmad, M. Z., Ahmad, J., Algahtani, M. S., Alali, A. S., Alsudir, S. A., Aodah, A. H., & Albarqi, H. A. (2022). Development of a curcumin-loaded lecithin/chitosan nanoparticle utilizing a Box-behnken design of experiment: Formulation design and influence of process parameters. *Polymers*, *14*(18), Article 3758. https://doi.org/10.3390/polym14183758